Pharm Res (2010) 27:2614–2623
DOI 10.1007/s11095-010-0257-9

RESEARCH PAPER

Real-Time UV Imaging of Nicotine Release from Transdermal Patch

Jesper Østergaard • Emil Meng-Lund • Susan Weng Larsen • Claus Larsen • Karsten Petersson • James Lenke • Henrik Jensen

Received: 21 June 2010 / Accepted: 19 August 2010 / Published online: 2 September 2010

ABSTRACT

Purpose This study was conducted to characterize UV imaging as a platform for performing *in vitro* release studies using Nicorette® nicotine patches as a model drug delivery system.

Methods The rate of nicotine release from 2 mm diameter patch samples (Nicorette®) into 0.067 M phosphate buffer, pH 7.40, was studied by UV imaging (Actipix SDI300 dissolution imaging system) at 254 nm. The release rates were compared to those obtained using the paddle-over-disk method.

Results Calibration curves were successfully established which allowed temporally and spatially resolved quantification of nicotine. Release profiles obtained from UV imaging were in qualitative agreement with results from the paddle-over-disk release method.

Conclusion Visualization as well as quantification of nicotine concentration gradients was achieved by UV imaging in real time. UV imaging has the potential to become an important technology platform for conducting *in vitro* drug release studies.

KEY WORDS diffusion · *in vitro* release · transdermal delivery · UV imaging

INTRODUCTION

In vitro release and dissolution testing constitutes an important activity in drug formulation development and quality control. For immediate-release oral solid dosage forms compendial disintegration and dissolution tests are available. Also, for modified-release formulations, including extended-release tablets, patches, and bead-type drug delivery systems, standard *in vitro* drug release methodologies are used in quality control and for formulation development purposes (1). In some cases, the employment of sufficiently discriminative *in vitro* release methods has led to the establishment of *in vitro–in vivo* correlations (2–4). The successful outcome of *in vitro* release studies may be inversely related to the complexity of the release and transport processes taking place at the site of administration (5). In the field of advanced drug delivery systems, the adequacy of *in vitro* drug release testing has to rely on identification of novel *in vitro* techniques allowing the transport and interactions of the drug substance taking place immediately next to the site of administration (within 100–500 μm) to be studied in more detail. Thus, there is a need for information-rich *in vitro* characterization methods to meet the increasing demands for efficient formulation development within the pharmaceutical industry. Imaging techniques providing spectrally, spatially, and temporally resolved information have shown to be particularly useful in this context (6–12).

Electronic Supplementary Material The online version of this article (doi:10.1007/s11095-010-0257-9) contains supplementary material, which is available to authorized users.

J. Østergaard (✉) · E. Meng-Lund · S. W. Larsen · C. Larsen · H. Jensen
Department of Pharmaceutics and Analytical Chemistry
Faculty of Pharmaceutical Sciences, University of Copenhagen
Universitetsparken 2
2100 Copenhagen, Denmark
e-mail: joe@farma.ku.dk

K. Petersson
New Products, LEO Pharma A/S
Ballerup, Denmark

J. Lenke
Paraytec Ltd.
York, UK

UV imaging is the ability to generate spatially and time-resolved images from the absorbance (transmittance) of UV light. Through the use of UV imaging, the intensity of light in the UV range passing through a volume element of a quartz cell as a function of position and time can be quantified (Fig. 1). Optimally, UV imaging technology may be applied for quantification of dissolved drug substance in the immediate vicinity of the drug delivery system and to record in real-time concentration *versus* time profiles (concentration gradients forming from the drug delivery system) in a movie format. Commercial UV imaging instrumentation has recently become available. Due to the small physical size of the UV imager, ease of data acquisition, and detection in the UV range which is optimal for most drug substances, UV imaging appears to constitute an interesting format for conducting *in vitro* drug release studies in formulation development, potentially providing additional detailed information on drug release kinetics and mechanisms.

The objective of the present study was to characterize UV imaging as a platform for conducting *in vitro* release studies. As a model drug delivery system, commercially available nicotine patches (Nicorette®) were investigated. Emphasis was put on evaluating the quantitative capabilities of the imager with respect to monitoring quantitatively in real time the formation and development of concentration gradients. The rate of nicotine release from 2-mm diameter patch samples into aqueous buffer solution was studied by UV imaging, and the release rates were compared to those obtained using the paddle-over-disk method.

Transdermal patches are used in nicotine replacement therapy, which is often the mainstay in the treatment for achieving smoking cessation (13–15). Nicotine is dissolved in the polymer matrix constituting the Nicorette® transdermal patch; thus, the formulation may be categorized as a monolithic solution (16). The release of nicotine from the Nicorette® patch into aqueous solution has been described as a polymer matrix diffusion-controlled process as indicated from the linear relationship between the amount released M_t and the square root of time $t^{\frac{1}{2}}$ (13,14).

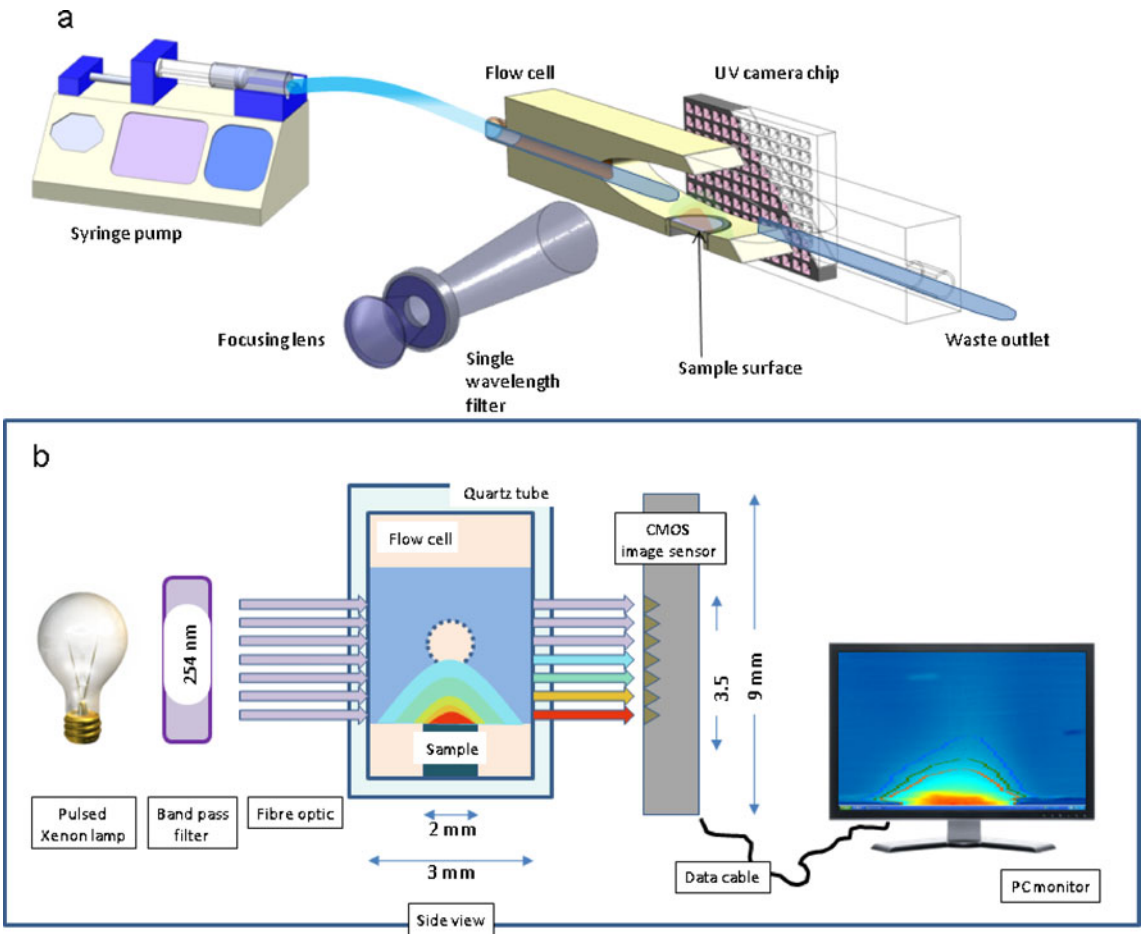

Fig. 1 Schematic representation of the UV imaging experimental setup.

MATERIALS AND METHODS

Materials

(-)-Nicotine was obtained from Sigma-Aldrich Co. (St. Louis, MO, USA). Nicorette® (5 mg/16 h (10 cm^2) and 15 mg/16 h (30 cm^2)) nicotine patches were obtained from Pfizer (Ballerup, Denmark). Sodium dihydrogenphosphate monohydrate and sodium hydroxide were obtained from Merck (Darmstadt, Germany). Purified water from a Milli-Q deionization unit (Millipore, Bedford, MA, USA) was used throughout.

The release media used was 0.067 M sodium phosphate, adjusted to pH 7.40 with 5 M sodium hydroxide. The nicotine standard solutions for calibration curves were prepared by suitable dilution of pure nicotine into the phosphate buffer.

A sharpened stainless steel cylinder (2 mm inner diameter; Actitube (Paraytec Ltd, York, UK)) was used for coring out samples of the nicotine patches. The cylinder also served as holder of the patch sample during UV imaging experiments.

UV Imaging Release Experiments

UV imaging was performed using an Actipix SDI300 dissolution imaging system (Paraytec Ltd.) with an Actipix flow-through-type dissolution cartridge. The detection area of the UV imager is 9 mm × 7 mm (1280 × 1024 pixels). The pixels (7 μm × 7 μm) were binned 4 × 4. The light source is a pulsed Xe lamp, and imaging was performed at 254 nm (band width 10 nm). Images were recorded (2.59 images per sec) and analyzed using Actipix D100 software version 1.3 (Paraytec Ltd.). The syringe pump was used for infusion of release media and nicotine standard solutions. The quartz cell (7.5 mm × 3.0 mm × 63 mm (H × W × L)) of the dissolution cartridge contained approximately 0.56 ml release media with the inserts in place.

The general procedure for UV imaging was as follows: dark images (I_0; lamp turned off for 10 s) and reference images (I_{ref}; 10 s) were recorded with the release cell filled with 0.067 M sodium phosphate buffer (pH 7.40); after 60 s of data collection, the recording was paused, and the nicotine patch sample mounted. During the reference period, a stainless steel cylinder was placed in the sample holder. After placing the nicotine patch sample, data collection was resumed, and the release cell was filled with buffer. The release experiments were conducted in stagnant release media (absence of flow) or using a flow-stopped-flow procedure. In the flow-stopped-flow mode, the lengths of the stopped-flow intervals were in the range of 3–10 min (starting with shorter intervals) intervened by 1-min periods where a flow rate of 2.0 $ml\,min^{-1}$ was applied. Uninterrupted imaging of the nicotine *in vitro* release experiments ($n=6$, from the same patch) was performed for 5 h at ambient temperature (20–23°C).

Calibration curves for the UV imager were constructed using 7 nicotine solutions: $4.9 \cdot 10^{-6}$, $9.7 \cdot 10^{-6}$, $4.9 \cdot 10^{-5}$, $1.9 \cdot 10^{-4}$, $4.9 \cdot 10^{-4}$, $7.8 \cdot 10^{-4}$, and $1.2 \cdot 10^{-3}$ M. Recording of UV images was performed while each of the standard solutions was infused for a period of 2 min at a flow rate of 2 $ml\,min^{-1}$. Buffer was infused before and after the series of nicotine solutions for 4 min in order to detect baseline drift. The infusion sequence for constructing the calibration curves (buffer, the 7 standard solutions, and buffer) was repeated 3 times. Conversion of pixel intensities into absorbance values (A) was done using the Actipix software based on Eq. 1:

$$A = \log\left(\frac{I_{ref} - I_0}{I_{sig} - I_0}\right) \tag{1}$$

where I_0, I_{ref}, and I_{sig} are the pixel intensity due to the dark current (electronic noise measured with the lamp turned off), pixel intensity measured with the 0.067 M phosphate buffer in the cell (reference signal), and pixel intensity measured during the experiment, respectively.

The Limit of Quantification (LOQ) for repeated injection of nicotine standard solutions was estimated from Eq. 2:

$$\mathrm{LOQ} = \frac{C}{AU} \cdot 10 \cdot SD \tag{2}$$

where C, AU, and SD are the concentration of the nicotine standard solution, the mean UV absorbance of the selected pixels and the standard deviation of the mean UV absorbance, respectively.

Paddle-Over-Disk Release Studies

The release experiments were performed at 32°C using a USP apparatus 5 (paddle over disk) (17). Nicorette® nicotine patches (15 mg/16 h; area 30 cm^2) were placed flat, 25 mm under the rotating paddle (100 rpm), in 500 ml release medium consisting of 0.067 M phosphate buffer (pH 7.40). The nicotine release experiments (in triplicate) were followed for 24 h, and at appropriate time intervals sample aliquots of 1 ml were withdrawn and replaced by 1 ml of the release medium. The amount of nicotine in the samples was quantified using UV spectrophotometry. A conventional double-beam UV–Vis spectrophotometer Shimadzu UV-1700 (Kyoto, Japan) was used to obtain UV spectrum, calibration curve and quantification of nicotine in the release experiments. Quartz cuvettes with a path length of 10 mm were applied (Hellma, Müllheim, Germany). The quantification was performed with a

wavelength at 254 nm (slit width 0.1 nm). The calibration curve for the double-beam spectrophotometer was constructed from 5 standard solutions of nicotine in the range $3.3 \cdot 10^{-6}$ to $3.8 \cdot 10^{-4}$ M. Each solution was measured three times.

Homogeneity of Patches

Using the sharpened stainless steel cylinder, 12 samples from the same patch were taken at random positions and placed in 1 ml of 0.067 M phosphate buffer for 48 h at ambient temperature. Subsequently, the amount of nicotine released from each sample was determined by UV spectrophotometry as described above. Three analyses were performed on each sample.

Diffusion Coefficient Determination by Taylor Dispersion Analysis

Taylor dispersion analysis was performed on an Agilent ^{3D}CE instrument (Agilent Technologies, Waldbronn, Germany) with an Actipix D100 UV area imaging detector (Paraytec Ltd., York, UK) for detection at two windows along the capillary as described elsewhere (18). The UV traces (214 nm) from each of the detection windows were recorded using Actipix software version 1.2. A fused silica capillary (Polymicro Technologies, Phoenix, AZ, USA), 75 μm inner diameter with a total length of 90 cm and lengths of 30 cm and 50 cm to the centre of first and second detection window, respectively, was used. The capillary was flushed with 0.067 M phosphate buffer, pH 7.4, for 2 min between injections. Injection of nicotine samples ($1 \cdot 10^{-3}$ M) was conducted by application of pressure (50 mbar for 7 s). The mobilization pressure applied to force the sample plug through capillary was 50 mbar with the phosphate buffer in the mobilization vial. The experiment was conducted at 23°C. Peak appearance time and temporal variance of the Gaussian-shaped peaks were obtained using the Actipix software. The diffusion coefficient was subsequently calculated from the Stokes-Einstein equation (18). Root mean square distances of nicotine diffusion $(x^2)^{\frac{1}{2}}$ were calculated according to

$$\left(x^2\right)^{\frac{1}{2}} = (2Dt)^{\frac{1}{2}} \tag{3}$$

Data Analysis

Quantification of nicotine release rates and cumulated release were a function of time. For each of the stopped flow intervals, the increase in absorbance of the active pixels was averaged for each image (time point). The amount of nicotine released at each time point in the stopped-flow intervals was calculated from the molar absorption coefficient, the size of the imaging area, and the light path (3.0 mm). Release rates were attained by fitting the stopped-flow release profiles to Eq. 4 (14,19,20).

$$M_t = k \cdot t^{\frac{1}{2}} \tag{4}$$

where M_t is the amount of nicotine released at time t, and k is the drug release flux. Plots of the release rate R as a function of time were fitted to Eq. 5:

$$R = \frac{1}{2} \cdot k \cdot t^{-\frac{1}{2}} \tag{5}$$

The cumulated nicotine release-time profiles for the entire release experiment were calculated from the flux rate constant obtained from Eq. 5 by insertion of k into Eq. 4.

RESULTS

Quantitative Performance of the UV Imager

UV imaging was performed in a parallel piped quartz cell with a light path of 3.0 mm; the area selected for imaging was 9.0 mm × 4.3 mm. In principle, this provides ~$5 \cdot 10^4$ individual UV spectrophotometers because 4×4 pixel binning was applied. Calibration curves for nicotine had to be constructed and the quantitative performance of the UV imager verified before taking up the *in vitro* release experiments. For this purpose, the phosphate buffer followed by a series of nicotine standard solutions was flowed through the release cell (2 mlmin^{-1}), while detection was performed at 254 nm. Fig. 2a shows pixel intensities over the imaged volume element (area) for a $8.0 \cdot 10^{-4}$ M nicotine solution. The conversion of pixel intensities into absorbance values was done using Eq. 1. From Fig. 2a, it is apparent that the light source does not provide the same intensity across the imaging area. The extent to which this is corrected for (Fig. 2b), by applying Eq. 1, was assessed by evaluating sub selections of pixels. Fig. 2c shows mean absorbance values as a function of concentration (and time) for pixel sub selections 1, 2, 3, and 4 obtained by flowing phosphate buffer and nicotine standards through the release cell (2 mlmin^{-1} for 2 min each). Using the plateau absorbance values for each nicotine concentration (Fig. 2c), the calibration curves shown in Fig. 2d were constructed. The calibration curves attained from the pixel sub-selections 1, 2, 3, and 4 were almost identical, and the slopes of the calibration curves were $7.23 \cdot 10^5$, $7.20 \cdot 10^5$, $7.27 \cdot 10^5$, and $7.42 \cdot 10^5$ (mAU M^{-1}) for pixel sub-selection 1, 2, 3, and 4, respectively. Selection 4 was slightly noisier and had higher absorbance values. From the slopes of 3 calibration curves (sub-selection 1), the molar absorp-

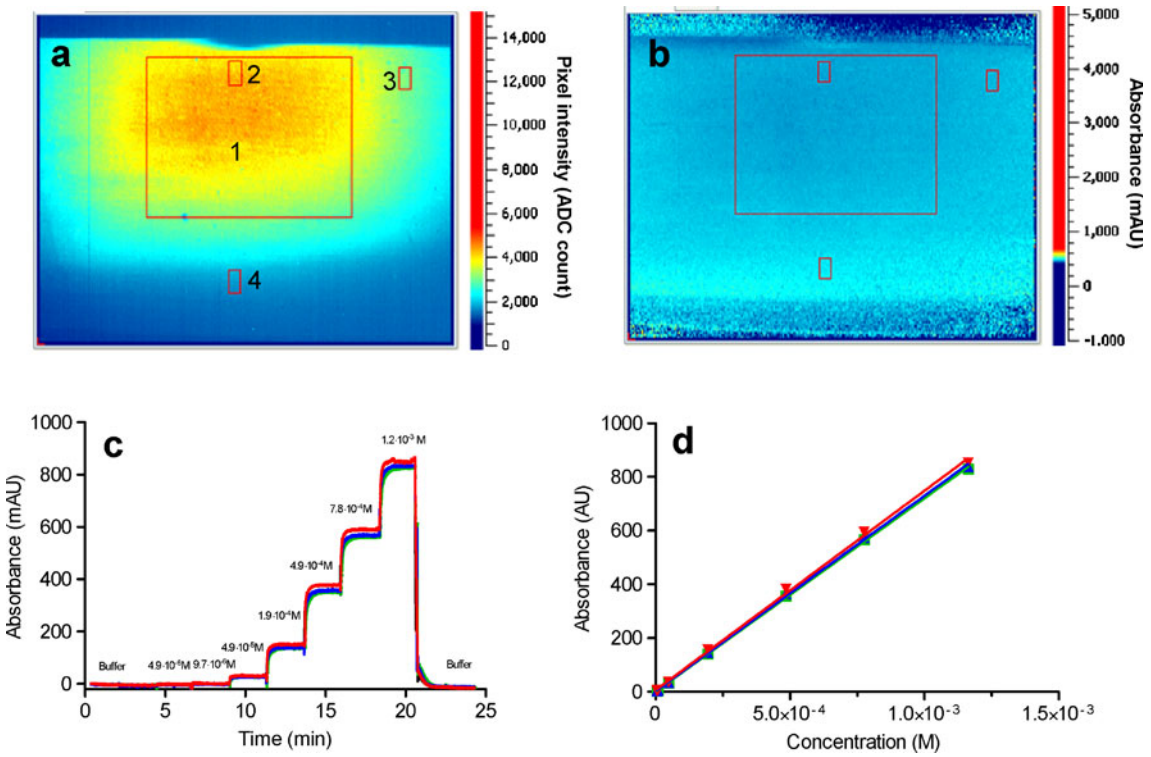

Fig. 2 Sample image of $8.0 \cdot 10^{-4}$ M nicotine in 0.067 M phosphate buffer, pH 7.4. (**a**) Pixel intensity (measure of transmittance). Pixel sub-selections 1, 2, 3, and 4 are marked with red color. (**b**) UV absorbance map attained from pixel intensities. (**c**) Average UV absorbance-time profiles for pixel sub-selections 1 (▬), 2 (▬), 3 (▬), and 4 (▬) obtained during construction of calibration curve by flowing nicotine standards through the release cell. (**d**) Calibration curves constructed from plateau absorbance values of panel (**c**) for pixel sub-selections 1, 2, 3, and 4.

tion coefficient of nicotine in phosphate buffer (pH 7.40) was determined: $\varepsilon_{254} = 2422 \pm 7$ M^{-1} cm^{-1} (mean ± SD (n=3)). For comparison, the molar absorption coefficient was also determined using a conventional double-beam UV spectrophotometer using similar experimental conditions: $\varepsilon_{254} = 2520 \pm 4$ M^{-1} cm^{-1} (mean ± SD (n=3)). The UV imaging nicotine calibration curve at 254 nm was considered linear within the investigated range. For six repeated instillations of buffer and $4.9 \cdot 10^{-6}$ M nicotine solution, the RSD of mean absorbance value was 10% (pixel sub-selection 1). The LOQ was estimated from Eq. 2 to $4.9 \cdot 10^{-6}$ M.

Monitoring of Concentration Gradients

The nicotine patch samples 2 mm in diameter were mounted in the UV imager parallel to the light path and in plane with the surface of the support constituting the wall of the release cell (Fig. 1). After positioning of the nicotine patch sample, the release cell was filled with 0.067 M phosphate buffer, pH 7.4, after which the flow was arrested. UV imaging was performed during this process and continued for up to 1 h. Fig. 3a–c shows the release and diffusion of nicotine into the stagnant volume of buffer in the release cell in form of UV absorbance maps at 254 nm. Intense red color indicates high absorbance values (concentrations). A video clip of the nicotine release-diffusion process can be found in the Supplementary Material (up to 3 min). Apparent concentration *versus* distance profiles corresponding to the bar centred relative to the patch sample for the images in Fig. 3a–c are shown in Fig. 3d. Through the use of Beer's law, the nicotine concentrations were obtained from the UV absorbance of each binned pixel, the light path (3 mm), and the molar absorption coefficient. Thus, Fig. 3 and the accompanying video clip, in real time, show the formation and development of a nicotine concentration gradient in stagnant phosphate buffer over time.

The diffusion coefficient of nicotine was determined using Taylor dispersion analysis (18) in 0.067 M phosphate buffer (pH 7.40) to $6.65 \cdot 10^{-10}$ m^2 sec^{-1} (RSD=2.9% (n=6)). From the diffusion coefficient, the root mean square distances (Eq. 3) of nicotine after 1, 2, and 3 min of diffusion were calculated to $2.8 \cdot 10^2$, $4.0 \cdot 10^2$, and $4.9 \cdot 10^2$ μm, respectively.

UV Imaging of Nicotine Release from Patch Samples

The nicotine patches are designed to release nicotine over a prolonged period of time (~16 h). The release of nicotine from the 2-mm diameter patch samples was followed for 5 h. A limitation in the software available prohibited experiments over longer periods of time. Efforts to quantify

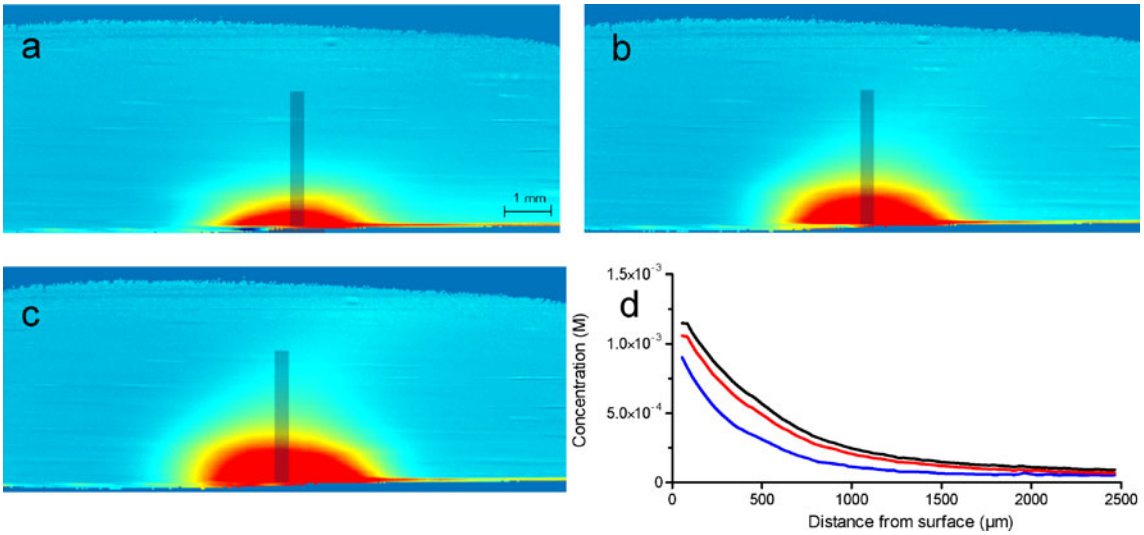

Fig. 3 Imaging of nicotine release and diffusion from Nicorette® patch sample under static conditions in 0.067 M phosphate buffer, pH 7.4. UV absorbance images obtained after (**a**) 1 min, (**b**) 2 min, and (**c**) 3 min. Panel (**d**) shows concentration-distance profiles (concentration gradients) corresponding to the bar in panels (**a**–**c**) at 1 (▬), 2 (▬) and 3 (▬) min.

the release of nicotine into a continuous flow by UV imaging were not successful. Presumably, detector sensitivity was insufficient to monitor the slow rate of nicotine release from the patch. Instead a flow-stopped-flow procedure was developed. A video clip of the first 23 min of a nicotine flow-stopped-flow release UV imaging experiment is supplied in the Supplementary Material. Fig. 4a shows the changes in the average UV absorbance at 254 nm of

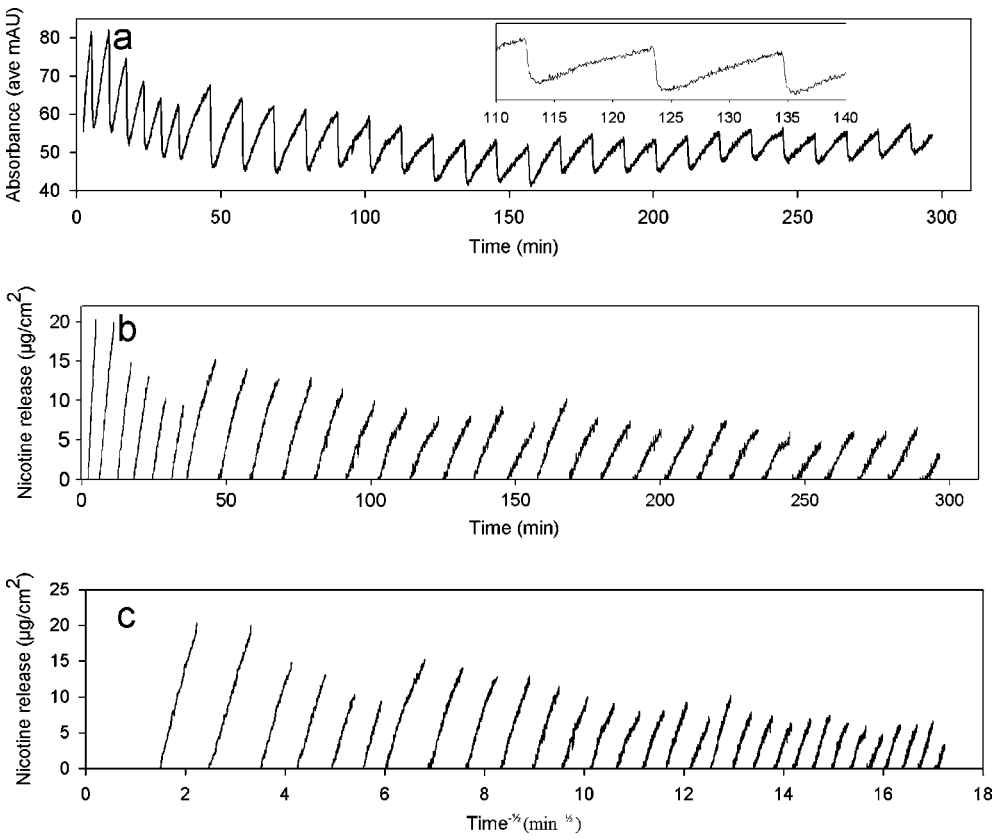

Fig. 4 Representative UV imaging flow-stopped-flow nicotine release experiment in 0.067 M phosphate buffer solution, pH 7.4. Nicorette® patch sample 2 mm in diameter. Panel (**a**) shows the average UV absorbance at 254 nm as a function of time. The amount of nicotine released as a function of time (**b**) and square root of time (**c**).

the whole imaging area over a 5 h period. Increases in average UV absorbance are observed in the time periods where the flow is stopped (3–10 min intervals); a step decrease in average absorbance to a base-line level is seen when a flow of 2 mlmin^{-1} is applied over a 1 min interval. The amount of nicotine released at a given time point in each of the stopped-flow periods was calculated from the increase in UV absorbance, the molar absorption coefficient, and the selected volume element (V=109 µl) of the imaging area (Fig. 4b). The calculations rely on the assumptions that the UV absorbance for each 4×4 pixels read is within the range of Beer's law and that nicotine does not diffuse out of the imaged volume element during the stopped-flow intervals. From Fig. 4, it is apparent that the rate of nicotine release decreases during the 5-h period. In Fig. 5a, the nicotine release rate R as a function of time t and $t^{-\frac{1}{2}}$ is shown for a representative patch sample. The release rate for each time point in Fig. 5a was determined from the slopes of the release profiles in Fig. 4c using Eq. 4. The cumulated amount of nicotine released from a representative patch sample as a function of time (Fig. 5b) was calculated using the release flux k obtained upon fitting the R *versus* time data in Fig. 5a to Eq. 5. Plots of the cumulated nicotine release *versus* the square root of time were linear (Fig. 5b insert). Fig. 6 shows the cumulated nicotine release profiles constructed from six flow-stopped-flow UV imaging experiments. The drug release flux (k) used for calculating the release profiles had a mean value of 24.2±3.7 µg cm^{-2} $min^{-1/2}$. By the end of the 5-h period, the calculated amount of nicotine released varied from 352 to 512 µgcm^{-2}. For comparison, 15.3±1.7 µg (486±53 µg cm^{-2} (n=12)) of nicotine was released from the patch samples into 1 ml of phosphate buffer after 48 h at room temperature.

Measurement of Nicotine Release Using Paddle Method

For comparison with the release profiles attained using UV imaging, the nicotine release from intact Nicorette® patches into phosphate buffer at 32°C was determined. The cumulated amount of nicotine released as a function of time is shown in Fig. 6. Plots of M_t against the square root of time were linear, and the release flux constant k was determined to be 14.3±0.6 µgcm^{-2} $min^{-1/2}$ (n=3). It is apparent that the release kinetics can be described by Higuchi kinetics.

DISCUSSION

Quantitative Performance of the UV Imager

A prerequisite for the development of UV imaging as a platform for performing *in vitro* release studies is that the spatially and time-resolved UV absorbance data can be attained and processed in a quantitative manner. Pixel intensities were automatically converted into absorbance values through Eq. 1. From Fig. 2a, it is apparent that the lamp energy is not uniform across the imaging surface. However, this was found to have only a minor effect on the UV absorbance values generated. This was demonstrated

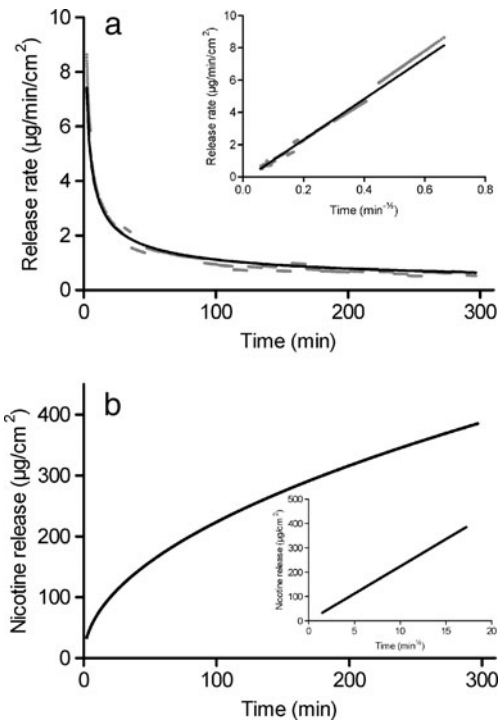

Fig. 5 Nicotine release rates as function of time (**a**) and the calculated cumulated nicotine release profile (**b**) obtained from a representative UV imaging flow-stopped-flow nicotine release experiment in 0.067 M phosphate buffer solution, pH 7.4. Nicorette® patch sample 2 mm in diameter.

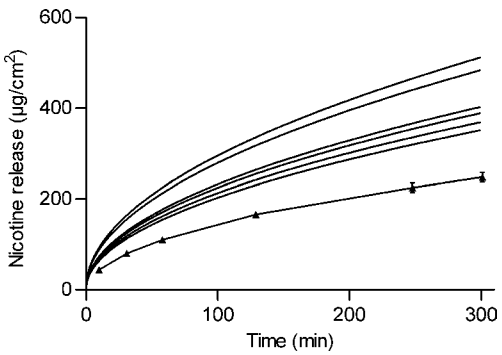

Fig. 6 Nicotine release profiles attained from UV imaging flow-stopped-flow experiments at 20–23°C and paddle-over-disk method at 32°C. UV imaging: 6 individual calculated cumulated nicotine release profiles. Paddle-over-disk (▲; mean ± SD (n=3)).

by the almost similar absorbance *versus* time profiles (Fig. 2c) and calibration curves (Fig. 2d) obtained from different pixel sub-selections. It was concluded that the molar absorption coefficient determined from pixel sub-selection 1 could be used to convert UV absorbance values read in the entire imaging area into nicotine concentrations with satisfactory accuracy and precision. This was of practical importance because entering of the molar absorption coefficient into the Actipix software allowed nicotine concentrations to be read directly from the UV images. Estimates of repeatability and LOQ were attained and found to be acceptable for the current purpose. Preconditions (fulfilled in the study) for the correct conversion of pixel intensities into analyte concentrations are that Beer's law is obeyed and that other UV absorbing species do not interfere with the quantification. For these reasons, 254 nm was selected as the detection wavelength rather than 200 or 214 nm in the nicotine release studies.

Monitoring of Concentration Gradients

Upon verification of the performance of the UV imager, nicotine patch samples (2 mm diameter) cored from Nicorette® transdermal patches were mounted in the release cell. While collecting the data, the release and diffusion of nicotine into the phosphate buffer release media was monitored real-time using the commercial software. The Supplementary Material provides sample video clips of the development of the nicotine concentration gradient with the time. Selected images and concentration *versus* distance profiles are shown in Fig. 3. The diffusion zone centred relative to the patch sample is almost symmetrical in Fig. 3. However, it has to be recognized that this type of experiment, where drug release occurs into stagnant release media, is very sensitive to movements, vibrations, and residual flow and turbulence within the cell. In contrast to most *in vitro* models, which have been designed to have a (well-defined) constant diffusion layer, the current setup is characterized by not having a constant diffusion layer thickness. Fig. 3 clearly shows that the diffusion layer thickness increases with time. This type of setup with natural convection only might be of relevance in relation to dermal and transdermals, such as ointments, creams, and patches, as well as delivery systems for parenteral administration, such as *in situ* suspension forming systems, stents and implants.

In principle, quantitative information in terms of, e.g., diffusion coefficients (in addition to release rates which are discussed below), can be extracted from the type of experiments outlined here. The ease of such exercises depends to a large extent, however, on the geometry of the experimental setup. With simple geometric setups, it may be sufficient to consider the release and diffusion in one dimension only. In relation to the design and geometry of the release cell, it has to be noted that the nicotine patch is 2 mm in diameter and that the light path is 3 mm in length. Thus, in the present case, some consideration is required; because the UV absorbance (concentration) determined is a value averaged over the entire light path, release occurs from a circular disk, and diffusion was not limited to one dimension. Tentatively, the release of nicotine and diffusion into solution was approximated with release from a slab. However, a poor fit between the data and the model was attained. Instead the root mean square distances for nicotine after 1, 2, and 3 min of diffusion were calculated for qualitative comparison to Fig. 3d. It is found that the apparent concentration *versus* distance profiles are compatible with the root mean square distances calculated from the diffusivity of nicotine. Even though a quantitative model was not developed, it is suggested that UV imaging combined with suitable release models can provide useful insights into the release behaviour of transdermal and dermal (monolithic solutions) drug delivery systems.

In Vitro Release of Nicotine: Comparison of UV Imaging to Paddle-Over-Disk

For UV imaging to become a versatile tool in drug release testing, it is imperative that quantitative release data can be attained. Therefore, nicotine release was investigated by the paddle-over-disk method in addition to the developed flow-stopped-flow release method. A simple approach was taken for the data analysis of the UV imaging data. The increase in absorbance of all the active pixels was used to determine the amount of nicotine released as a function of time for all the stopped-flow intervals (Fig. 4a and b). Since it was known that the Nicorette® patch can be categorized as a polymer matrix diffusion-controlled system (13,14), the amount released was plotted against $t^{\frac{1}{2}}$. Determination of the flux rate constant for each stopped-flow interval subsequently led to the determination of nicotine release rate as a function of time (Fig. 5a) as well as the cumulated nicotine release (Figs. 5b and 6). For drug delivery systems for which prior knowledge of the release kinetics is not available, it is suggested that drug release in the stopped-flow intervals can be fitted to polynomial or exponential functions, thus allowing release rates to be determined.

Equation 4 was developed for the release of active from a monolithic solution into a sink (14,19,20) and, therefore, is not directly applicable to the stopped-flow situation. The build-up of nicotine at the patch sample-buffer interface is readily visualized by the UV images. Apparently, this aqueous diffusion barrier does not significantly decrease the nicotine release from the patch samples. It is assumed

that the flow-stopped-flow procedure provides release conditions approximating those of a sink. The contribution of natural convection to dissolution rates in drug dissolution studies has been discussed previously (21–23). However, the experimental data obtained do not allow discussion of such possible effects (believed to be small) on drug release rates due to density gradients.

Release profiles obtained from UV imaging were associated with larger variability (RSD = 16% (n = 6)) relative to those obtained by the disk-over-paddle method as apparent from the release flux constant. It is suggested that this might be related to difficulties in placing the patch sample in the cylinder in a repeatable manner. However, uneven distribution of nicotine among the 2-mm diameter patch samples may also be a contributing factor as indicated from the measurement of the amount of nicotine released from 12 patch samples (RSD = 11% (n = 12)) into phosphate buffer.

The release profiles constructed from the UV imaging experiments were qualitatively similar to those obtained using the paddle-over-disk method (Fig. 6); both sets of profiles could be described by Higuchi kinetics. A slower release from UV imaging experiments might have been expected due to the temperature difference (20–23°C *vs.* 32°C). However, this was not the case as shown by the release flux constants (k) of 24.2 ± 3.7 $\mu g cm^{-2}$ $min^{-1/2}$ and 14.3 ± 0.6 $\mu g cm^{-2}$ $min^{-1/2}$ obtained using the UV imager and the paddle-over-disk method, respectively. The reasons for this apparent discrepancy are not clear. A potential cause may be an edge effect due to the sampling of the nicotine patch (increased release from the edge of the sample patches). Also, in case the side of the cylindrical patch sample is partly exposed to the release medium, an increased nicotine release must be expected due to the augmented surface area of the patch. The area available for nicotine release will be increased by 20% and 100% in case the exposed heights of the cylindrical patch samples are 0.1 mm and 0.5 mm, respectively. For reference, previous studies of nicotine release from Nicorette® patches into aqueous solution provided release fluxes of 21.9 $\mu g cm^{-2}$ $min^{-1/2}$ (Valia-Chien permeation cell, pH 5.0 at 37°C) (14) and 10.7 $\mu g cm^{-2}$ $min^{-1/2}$ (disk over paddle, dilute HCl at 32°C) (13). Overall, the nicotine flow-stopped-flow experiments conducted demonstrate the potential applicability of UV imaging for *in vitro* release studies. In relation to dermal and transdermal drug delivery, replacement of the nicotine patch with gels or ointments can be envisioned. Other formulation types may be accommodated in the cylinders or similar retainers or placed directly in the imaging area, allowing detailed studies of drug release to be performed. It is a prerequisite, however, that the drug delivery system is not compromised by the sampling procedure.

CONCLUSION

The present investigation constitutes a first step toward implementing UV imaging as platform for conducting *in vitro* release studies. Calibration curves were successfully established which allowed temporally and spatially resolved quantification of nicotine. Visualization of the formation and development of concentration gradients within the release cell were easily achieved as the UV imager facilitated the detection and quantification of the drug substance (nicotine) adjacent to the applied formulation (nicotine patch sample) in real time. Nicotine release profiles obtained from UV imaging were in qualitative agreement with paddle-over-disk release data. However, the nicotine release rates determined using UV imaging were higher than those attained using the paddle over disk; an edge effect is suggested to the cause for this apparent discrepancy. UV imaging has the potential to become a versatile research tool in *in vitro* drug release testing as well as in visualisation of drug transport processes, e.g., diffusion.

ACKNOWLEDGEMENTS

This work was supported by the Danish Medical Research Council. JOE and EML thank LEO Pharma for financial support. JL thanks Yorkshire Forward for support through R&D Grant, project number YHF/02803/RD09.

REFERENCES

1. Clark BC, Dickinson PA, Pyrah IT. *In vitro/in vivo* release from injectable dispersed systems. In: Burgess DJ, editor. Injectable dispersed systems. Formulation, processing, and performance. Boca Raton: Taylor and Francis; 2005. p. 125–57.
2. Dutta S, Qiu Y, Samara E, Cao G, Granneman GR. Once-a-day extended-release dosage form of divalproex sodium III: development and validation of a level A *in vitro-in vivo* correlation (IVIVC). J Pharm Sci. 2005;94:1949–56.
3. Soto E, Haertter S, Koenen-Bergmann M, Staab A, Troconiz IF. Population *in vitro–in vivo* correlation model for pramipexole slow-release oral formulations. Pharm Res. 2010;27:340–9.
4. Takka S, Sakr A, Goldberg A. Development and validation of an *in vitro–in vivo* correlation for buspirone hydrochloride extended release tablets. J Control Release. 2003;88:147–57.
5. Larsen C, Larsen SW, Jensen H, Yaghmur A, Østergaard J. Role of *in vitro* release models in formulation development and quality control of parenteral depots. Expert Opin Drug Deliv. 2009;6:1283–95.
6. Richardson JC, Bowtell RW, Mäder K, Melia CD. Pharmaceutical applications of magnetic resonance imaging (MRI). Adv Drug Deliv Rev. 2005;57:1191–209.
7. Kempe S, Metz H, Mäder K. Application of electron paramagnetic resonance (EPR) spectroscopy and imaging in drug delivery research—chances and challenges. Eur J Pharm Biopharm. 2010;74:55–66.
8. Metz H, Mäder K. Benchtop-NMR and MRI—a new analytical tool in drug delivery research. Int J Pharm. 2008;364:170–5.

9. Bobiak JP, Koenig JL. Regions of interest in FTIR imaging applications: diffusion of nicotine into ethylene-co-vinyl acetate films. J Control Release. 2005;106:329–38.
10. Rafferty DW, Koenig JL. FTIR imaging for the characterization of controlled-release drug delivery applications. J Control Release. 2002;83:29–39.
11. Young PM, Nguyen K, Jones AS, Traini D. Microstructural analysis of porous composite materials: dynamic imaging of drug dissolution and diffusion through porous matrices. AAPS J. 2008;10:560–4.
12. Zeitler JA, Gladden LF. *In vitro* tomography and non-destructive imaging at depth of pharmaceutical solid dosage forms. Eur J Pharm Biopharm. 2008;71:2–22.
13. Olivier J-C, Rabouan S, Couet W. *In vitro* comparative studies of two marketed transdermal nicotine delivery systems: Nicopatch® and Nicorette®. Int J Pharm. 2003;252:133–40.
14. Ho H, Chien YW. Kinetic evaluation of transdermal nicotine delivery systems. Drug Dev Ind Pharm. 1993;19:295–313.
15. Lin S, Ho H, Chien YW. Development of a new nicotine transdermal delivery system: *in vitro* kinetics studies and clinical pharmacokinetic evaluations in two ethnic groups. J Control Release. 1993;26:175–93.
16. Baker R. Controlled release of biologically active agents. New York: Wiley; 1987.
17. Shah VP, Tymes NW, Ment W, Shelly JP. Collaborative study results of a dissolution test procedure developed by FDA for nitroglycerin transdermal delivery systems. Pharmacop Forum. 1988;14:3458–62.
18. Østergaard J, Jensen H. Simultaneous evaluation of ligand binding properties and protein size by electrophoresis and Taylor dispersion in capillaries. Anal Chem. 2009;81:8644–8.
19. Higuchi T. Physical chemical analysis of percutaneous absorption process from creams and ointments. J Soc Cosmet Chem. 1960;11:85–97.
20. Higuchi WI. Analysis of data on the medicament release from ointments. J Pharm Sci. 1962;51:802–4.
21. Stevens LE, Missel PJ. Impact of density gradients on flow-through dissolution in a cylindrical flow cell. Pharm Dev Technol. 2006;11:529–34.
22. D'Arcy DM, Liu B, Bradley G, Healy AM, Corrigan OI. Hydrodynamic and species transfer simulations in the USP 4 dissolution apparatus: considerations for dissolution in a low velocity pulsing flow. Pharm Res. 2010;27:246–58.
23. D'Arcy DM, Corrigan OI, Healy AM. Evaluation of hydrodynamics in the basket dissolution apparatus using computational fluid dynamics-dissolution rate implications. Eur J Pharm Sci. 2006;27:259–67.